Theor Chem Acc (2011) 128:663–673
DOI 10.1007/s00214-010-0800-0

REGULAR ARTICLE

A density functional theory study of the 'mythic' Lindlar hydrogenation catalyst

M. García-Mota · J. Gómez-Díaz · G. Novell-Leruth · C. Vargas-Fuentes · L. Bellarosa · B. Bridier · J. Pérez-Ramírez · N. López

Received: 6 July 2010 / Accepted: 16 August 2010 / Published online: 7 September 2010

Abstract A Lindlar catalyst is a popular heterogeneous catalyst that consists of 5 wt.% palladium supported on porous calcium carbonate and treated with various forms of lead and quinoline. The additives strategically deactivate palladium sites. The catalyst is widely used for the partial hydrogenation of acetylenic compounds in organic syntheses. Alkyne reduction is stereoselective, occurring via *syn* addition to give the *cis*-alkene. Even if it has been employed for about 60 years, there is a lack of molecular level understanding of the Lindlar catalyst. We have applied density functional theory simulations to understand the structure and the nature of the interplay between the multiple chemical modifiers in the Lindlar catalyst. Indeed, the poisons influence different parameters controlling selectivity to the alkene: Pb modifies the thermodynamic factor and hinders the formation of hydrides, while quinoline isolates Pd sites thus minimizing oligomerization.

Keywords Hydrogenation · Acetylenic compounds · Lindlar catalyst · Selectivity · DFT

Published as part of the special issue celebrating theoretical and computational chemistry in Spain.

M. García-Mota · J. Gómez-Díaz · G. Novell-Leruth · C. Vargas-Fuentes · L. Bellarosa · N. López (✉)
Institute of Chemical Research of Catalonia (ICIQ), Avgda. Països Catalans 16, 43007 Tarragona, Spain
e-mail: nlopez@iciq.es

B. Bridier · J. Pérez-Ramírez
Institute for Chemical and Bioengineering, Department of Chemistry and Applied Biosciences, ETH Zürich, HCI E 125, Wolfgang-Pauli-Strasse 10, CH-8093 Zürich, Switzerland

1 Introduction

Heterogeneous catalysis has been the main contributor to the development of chemical industry development over the last century. Those catalysts are complex systems that contain a multiple set of ingredients; most commonly, they are presented in the form of solids and are ubiquitous in chemical and petrochemical transformation processes. Unlike the study of homogeneous catalysts and enzymes, the structure and composition of heterogeneous catalyst is very difficult to characterize. Therefore, the complementary use of computational tools based on density functional theory (DFT) and experiments has shown to improve our knowledge of the catalytic phenomena. The type of simulations required for these studies (based on DFT and periodic boundary conditions) is computationally highly demanding and, only in the last two decades, reliable computational tools and enough computer power to perform these simulations has been achieved. Indeed, the theoretical study of heterogeneous catalysis has provided guidelines to improve activity; however, this might not be enough when more industrially relevant problems are addressed.

The development of selective processes is the key for the research in the chemical industry in the twenty-first century [1]. Sharp reactions are a must to achieve eco-efficient alternatives to existing processes. A large fraction of reactions, in the production of bulk chemicals, fine chemicals, and pharmaceuticals, corresponds to selective hydrogenations [2, 3]. Hydrogenation reactions can involve a single unsaturated reactant that is then partially hydrogenated, multifunctionalized molecules, and/or complex mixtures presenting more than a single active species where only one of the reactants or functional groups should be partially hydrogenated. Selectivity can be classified in three different terms: selectivity to a reaction, to a reactant,

and to a product [4]. For partial alkyne hydrogenations, all these selectivities are required: namely stopping the hydrogenation process at the thermodynamically metastable alkene (product selectivity), eliminating the competition of different substrates for the catalyst (reactant selectivity), and blocking oligomerization reactions (reaction selectivity). Recently, our research efforts aimed at establishing links between material and pressure gaps for the gas-phase hydrogenation of alkyne + alkene mixtures and also the differences between homogeneous and heterogeneous catalysis for this particular type of reactions [5, 6]. The catalysts in both hydrorefining (i.e., gas-phase alkyne hydrogenation in alkene cuts of steam crackers) and the hydrogenation of acetylenic compounds in fine chemistry are based on palladium. However, the preparation of both catalysts and the conditions at which they run differ substantially.

The adsorption and selective hydrogenation of alkynes versus that of alkenes have been considered as a model reaction and have been subject to several theoretical studies mostly concentrated on the properties of clean palladium surfaces [7] and alloys [8]. Recently, the role of the formation of different phases, their correlation with the activity and selectivity and the effect of selectivity moderators have been investigated [9]. Attempts to identify more selective catalysts by means of theoretical calculations have also been performed [10]. In particular, for NiZn alloys a complete quenching of the over-hydrogenation route was proposed [10].

Alkyne hydrogenation in C2 and C3 cuts is widely implemented downstream of the steam crackers [3]. The main aim is to selectively reduce the amount of ethyne–propyne in the presence of ethene and propene-rich streams. This is done to increase the purity of these feeds to meet the strict demands (few ppm of the alkyne) of the polymerization units. The particular specifications of the catalyst of choice depend on the position in the plant, which determines the composition of the mixture (namely the hydrogen-to-alkyne ratio). A general catalyst contains very small amounts of Pd (<0.05 wt.%), supported on low-surface area alumina and with metal promoters (Ag, Au) and selectivity modifiers, mainly CO, see Table 1.

In fine chemistry, the Lindlar catalyst is stereotypic for hydrogenation of acetylenic compounds in the liquid phase [11, 12], see Table 1. This well-established catalyst contains up to 5 wt.% Pd supported on either $CaCO_3$ or $BaSO_4$. In the preparation, a solution of 5 wt.% of $Pb(OAc)_2$ is added to the initial catalyst to deactivate it. Then, the system is heated at low temperature (95 °C), and it is likely that the organic moiety is eliminated and some form of metallic lead deposit appears [13, 14]. It is well known that Pb and Pd do form solid solutions [15, 16], and studies on the interaction of Pb films with Pd(111) surfaces

Table 1 Comparison between the hydrogenation catalyst in hydrorefining units and the Lindlar catalyst

	Hydrorefining catalyst	Lindlar catalyst
Substrate	Ethyne, propyne	Long chain alkynes
Medium	Gas phase or liquid phase	Liquid phase
Pd content (%)	0.01–0.05	1–5
Second metal	Ag, Au, etc.	Pb, Bi, Cu
Selectivity modifier	CO	Quinoline
Support	Al_2O_3	$CaCO_3$, $BaSO_4$
Temperature	RT-350 K	RT
Solvent	None	Benzene, toluene, methanol
Regioselectivity	–	*cis*
p_{H2}	Up to 20 bar	1–10 bar
Operation	Continuous	Batch

demonstrate that formation of alloys is favored [17]. It has been suggested that a surface alloy with composition Pd_3Pb is formed, as the active species of the Lindlar catalyst [18], although the real surface stoichiometry of the material is not clear. In addition, penetration of Pb toward the bulk has been also put forward [13, 19, 20]. The rearrangement of Pd particles, when Pb is incorporated in the catalyst has also been suggested in the literature [21]. Alternative metals to Pb suggested in the first report by Lindlar were Bi and Cu [11]. Then, a second kind of modifier, a molecule with a strong interaction to the surface is added to the catalyst. Usually, these molecules are organic compounds possessing oxygen, sulfur, phosphorous, or nitrogen heteroatoms. The ratio of an efficient modifier to the substrate is in the range 0.01–1 mol% [22]. In the Lindlar catalyst, usually quinoline ($C_{11}H_{11}N$), is employed, although piperidine and 2,2′-(ethylenedithio)diethanol have been suggested too [12]. Quinoline has been proposed to: (1) compete with alkynes for the adsorption to the surface, (2) to inhibit alkene surface interactions [23], and (3) to reduce isomerization processes. Moreover, quinoline is thought to act as an electron donor to the surface and then modifies the polarization of the Pd–H bond [24].

In summary, in the Lindlar catalyst the Pd particles are likely to contain Pb as a dopant and to be poisoned by the N-containing organic rings. The Lindlar catalyst works at room to medium temperature and deactivates at higher temperatures. It is usually employed with organic solvents, (i.e., benzene and toluene), and when reactants are not soluble in this media, methanol can be employed. Selectivity results from the Lindlar catalyst are exceptional in the competition of alkyne and alkene groups and more than 85% is routinely obtained [11]. In addition, for complex substrates mainly *cis* insertion is observed. Thus, the Lindlar catalyst provides also some degree of regio-

selectivity. However, usually these processes are carried out in batch reactors and the selectivity is found to depend on the reaction time. At very long residence times, the preference to the *cis* is smoothed out and some degree of alkene hydrogenation can also be observed.

In order to understand how the Lindlar catalyst works and why it is so selective the comparison to what is known about hydrogenation catalysts can provide a lot of insight. Previous investigations on the hydrogenation of C2 and C3 cuts and the careful comparison of experimental and theoretical work have clarified the issue. We have explored different aspects regarding the gas-phase hydrogenation of alkynes in the presence of alkenes for different metals including Au [25], Ni and Cu [26], ternary Cu–Ni–Fe [27], and the interplay between different phases and the selectivity on Pd [9]. The three main controllers of the alkene selectivity are as follows:

1. *Thermodynamic selectivity*, this is the ability to adsorb preferentially only the alkyne moieties in the presence of any other functional group. This is the only controlling factor in Au nanoparticle-based catalysts.
2. *Inability to form a hydride phase*, hydrides overhydrogenate adsorbed moieties due to the presence of high potential sub-surface H species. Those present a smaller kinetic demand than the surface counterpart and thus invalidate the thermodynamic control. The catalyst of choice, Pd, has a large versatility in the formation of hydrides and thus, at high hydrogen-to-alkyne ratios, the performance of the Pd catalyst alone is extremely poor.
3. *Definition of small ensembles.* Two of the competing routes in the process involve the activation of H atoms toward the reactive moiety or, alternatively, the formation of C–C bonds. The ensembles required for the second reaction are larger than those of hydrogenation and thus are detrimental for selectivity. Moreover, oligomers can block the active sites. Therefore, reducing oligomerization is linked with the control of the ensemble size.

Our aim in the present work is to understand how the Lindlar catalyst deals with the points described above: thermodynamic factors, hydride formation and active ensembles. The 'mythic' Lindlar catalyst has been industrially applied for around 60 years; it is still used in natural product syntheses (like A vitamin) and remains the most popular catalyst for the partial hydrogenation of acetylinic compounds [12, 28]. Surprisingly, the reasons for the outstanding selectivity are still not well grounded. For instance, the study of the co-metal effect has been the subject of some investigations but a complete picture has not yet emerged [29]. There is a lack of studies that can unravel at the molecular level the role of the various ingredients in the Lindlar catalyst. This is precisely the aim of the present work, to give a rational understanding of the modifiers in Lindlar-type catalysts by comparison with pure palladium. In order to do this, the stability, activity, and selectivity properties of both Pd and a series of systems of increasing complexity (Pd–Pb alloys, Pd–quinoline and Pd–Pb–quinoline systems) that represent the Lindlar catalyst have been studied. To analyze the thermodynamic and kinetic factors of the hydrogenation process we have employed the simplest alkyne–alkene pair. This is supported by our previous calculations that indicate the similarities for C2 and C3 compounds for the Pd case.

2 Computational details

We have employed density functional theory applied to slabs with the VASP code [30]. The energies have been obtained through the PW91 version of the exchange and correlation functional [31]. The inner electrons have been represented through PAW pseudopotentials [32], while the valence electrons have been expanded in plane waves with a cut off energy of 400 eV. With this set up, the cell parameter for Pd was found to be 3.966 and 5.023 Å was obtained for Pb. The (111) surface has been employed for the reactivity studies, since this is the one showing the lowest energy for fcc metals. The slabs contain four layers in a $p(2 \times 2)$ reconstruction for the hydrogen formation and have been extended to six layers for the Pb solubility studies. In that case, a single Pd atom was substituted by Pb. These systems are denoted as Pb@Pd. Islanding was computed in a $p(3 \times 3)$ configuration with two Pb atoms on the surface. For the adsorption of quinoline on both Pd clean and Pb@Pd systems, a larger supercell with a $p(4 \times 4)$ reconstruction was employed, denoted Pd–Q_{Pd} and Pb@Pd–Q_{Pd}. In the second case, the amount of Pb was taken as either 0.25 or 0.0625 ML. The vacuum space interleaving the different slabs was set to >10 Å. The *k*-point sampling was performed with the Monkhorst–Pack [33] scheme with $5 \times 5 \times 1$ points for the small cell, and $3 \times 3 \times 1$ for the larger ones. To illustrate the decoration at steps, we have employed a Pd(211) cut with a (3×1) reconstruction and nine layers, the *k*-point sampling being $3 \times 3 \times 1$. These computational settings have been demonstrated to produce energies that are converged by 0.02 eV. In Fig. 1, a summary with all the models employed in the present calculations is shown.

As a representative model for the alkyne–alkene pair, we employed the smallest possible hydrocarbons: ethyne and ethene. In previous studies, we have seen how thermodynamic and kinetic properties of the hydrogenation reaction are similar for C2 and C3, although other properties, i.e., carbide formation, are a strong function of the

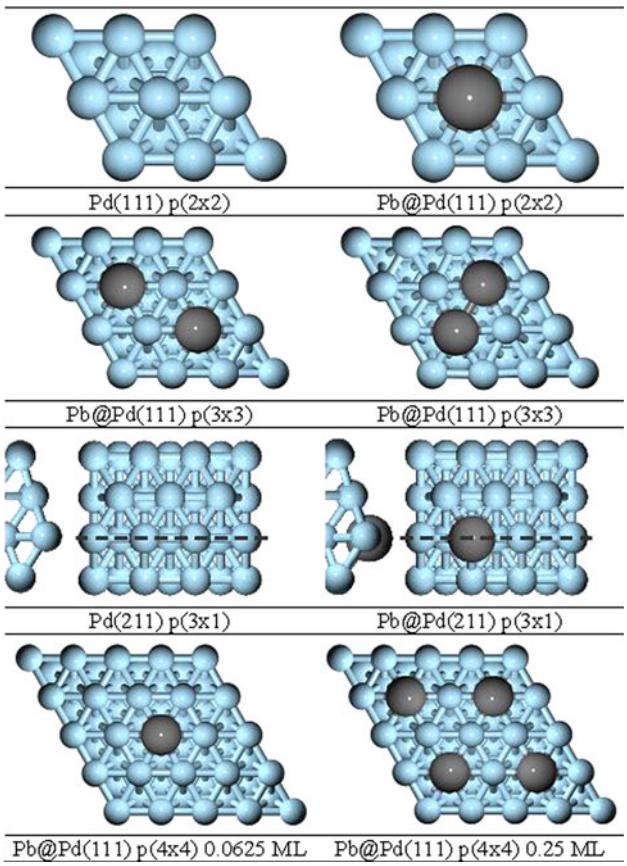

Fig. 1 Models for the different surfaces employed in the calculations. *Blue spheres* represent Pd and *gray* Pb. The *lines* indicate the edge for the step models

number of carbon atoms [9]. Adsorption was performed on one side of the unit cell and both the adsorbate and two upper layers were allowed to relax (z-direction). To determine the transition states CI-NEB calculations [34] were performed.

3 Results

3.1 The Pd–Pb system

The Pd–Pb system forms solid solutions with different compositions and structure [15]. In particular, at low Pb concentration, a solid solution where Pb substitutes Pd has been described. We have calculated the solubility for Pb impurities and the corresponding segregation profile for Pb in the Pd lattice. The energy profile is shown in Fig. 2. The solubility was calculated as:

$$E_{\mathrm{sol}} = E_{\mathrm{Pb@Pd}}^{(2\times2-6\mathrm{layer})} + E_{\mathrm{Pd(bulk)}} - E_{\mathrm{Pd}}^{(2\times2-6\mathrm{layer})} - E_{\mathrm{Pb(bulk)}} \quad (1)$$

where $E_{\mathrm{Pb@Pd}}^{(2\times2-6\mathrm{layer})}$ is the energy of the Pd slab with a substituted Pb atom, $E_{\mathrm{Pd(bulk)}}$ and $E_{\mathrm{Pb(bulk)}}$ are the corresponding bulk energies per atom for both metals, and $E_{\mathrm{Pb}}^{(2\times2-6\mathrm{layer})}$ the energy of the Pd slab. From Eq. 1, the substitution of Pb in the Pd lattice at the bulk position (L-3) is exothermic by 1.12 eV. Therefore, the formation of the Pb–Pd bond is more favorable than the Pb–Pb one and the solubility of Pb atoms is very likely considering also the contribution from configurational entropy [35]. We have also calculated the segregation energy to assess whether surface or bulk positions are more likely for the Pb impurities. The segregation energy has been calculated as follows:

$$E_{\mathrm{seg}} = E_{\mathrm{Pb(L-X)@Pd}}^{(2\times2-6\mathrm{layer})} - E_{\mathrm{Pb(L-3)@Pd}}^{(2\times2-6\mathrm{layer})} \quad (2)$$

where $E_{\mathrm{Pb(L-X)@Pd}}^{(2\times2-6\mathrm{layer})}$ is the energy for the impurity in the position L-X and L-3 represents the impurity sitting at the bulk. Calculations indicate the likely segregation of Pb toward the surface, see Fig. 2. The energy gain is 0.79 eV with respect to Pb in the bulk position. Surface Pb atoms are relaxed toward the vacuum by 0.227 Å. In addition, the Lindlar preparation method described in the Introduction will also promote Pb impurities to stay on the surface and thus surface impurity models and near-surface ones will be employed as the most likely structures under reaction conditions. A third aspect concerns the formation of Pb islands when considering impurities in the alloy. Island formation has been calculated as follows:

$$E_{\mathrm{isl}} = E_{\mathrm{Pb2@Pd}}^{(3\times3-4\mathrm{layer})} - E_{\mathrm{Pb+Pb@Pd}}^{(3\times3-4\mathrm{layer})} \quad (3)$$

where $E_{\mathrm{Pb2@Pd}}^{(3\times3-4\mathrm{layer})}$ is the energy of a Pb dimer on the Pd surface and $E_{\mathrm{Pb+Pb@Pd}}^{(3\times3-4\mathrm{layer})}$ is the energy of separated atoms in

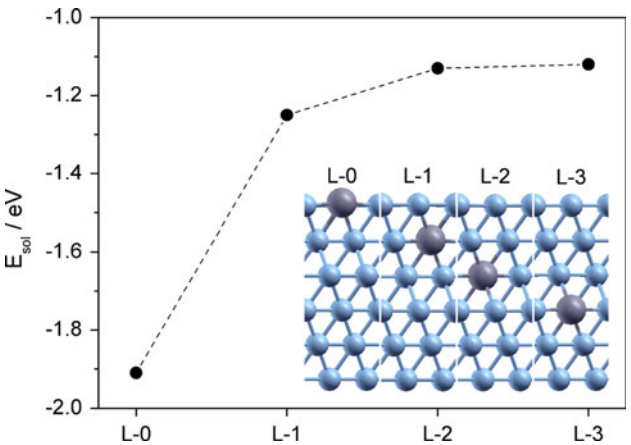

Fig. 2 Solubility energy of a Pb impurity in Pd(111). The inset indicates the positions of the lead atom in the palladium slab. Same color code as in Fig. 1

the same supercell. Pb islanding is endothermic by 0.6 eV and thus isolated Pb atoms are more likely on the surface.

A final aspect regarding the formation of the alloy is the preferential adsorption of Pb at step Pd sites. Indeed, competing reactions such as *cis–trans* isomerization and bond shift isomerization are more likely to occur on rough surfaces, i.e., rich in steps and kinks [36], and there have been some claims that the selective poisoning by Pb of these sites can be at least partially responsible for the enhanced selectivity [37, 38]. We have investigated this aspect by calculating the solubility at the steps.

$$E_{\text{step}} = E^{(3\times1-9\text{layer})}_{\text{Pb-step@Pd}} + E_{\text{Pd(bulk)}} - E^{(3\times1-9\text{layer})}_{\text{Pd-step}} - E_{\text{Pb(bulk)}} \quad (4)$$

where $E^{(3\times1-9\text{layer})}_{\text{Pb-step@Pd}}$ is the energy of the Pb impurity at the step site, $E^{(3\times1-9\text{layer})}_{\text{Pd-step}}$ the energy of the clean Pd step, and $E_{\text{Pd(bulk)}}$ and $E_{\text{Pb(bulk)}}$ the bulk energies per atom of Pd and Pb, respectively. Then, compared to an impurity in the terrace, Pb atoms at the step are more stable by 0.37 eV.

The electronic structure of Pd surfaces and Pb@Pd alloys is described in Fig. 3 through the Projected Density Of States, PDOS. The top figure illustrates the reference system, Pd slab. The bands for bulk and surface Pd atoms are clearly shown and the corresponding *d*-band structures indicate the presence of lower states for the fully coordinated Pd bulk atoms. The *d*-band center [39] for the bulk Pd is placed at 1.76 eV below the Fermi level while the corresponding parameter for Pd atoms on the pure surface is closer to the Fermi level, 1.41 eV. As shown in Fig. 3, the Pd surface layer and in particular the *d*-band is modified by the presence of Pb in the alloys. Upon the formation of the Pb@Pd alloy, the *d*-bands of the Pd atoms are shifted downwards by 0.16 eV. In turn, the Pb levels (only *s* and *p* states are plotted in Fig. 3) show a deep band at about −10 eV and a broad band crossing the Fermi level. Thus, the electronic structure analysis indicates that Pd atoms at the Pb@Pd structures are less reactive than the clean surface. This means that the surface is less prone to adsorb incoming alkyne or alkene molecules.

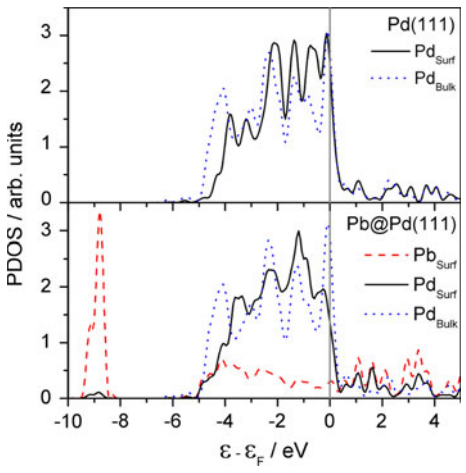

Fig. 3 Projected Density of States for Pd (*top*) and Pb@Pd (*bottom*) alloys. The *black line* represents the states for a surface Pd atom, *blue dotted* those of the bulk and *red dashed* the Pb states

3.2 Hydride and carbide formation in Pd and Pb@Pd

Pd is known to form different phases depending on the environment. Hydrides [40] are formed at room temperature at pressures as low as 0.024 atm [41]. Carbides come from the decomposition of organic molecules as indicated by Honkala et al. [42–45] and sit at octahedric sites in the subsurface region. In particular, this phenomenon is important since both carbides and hydrides are the key to control the selectivity of the catalyst [46, 47].

H_2 dissociation is known to happen even at high coverage with small energy requirements [48, 49]. The simplest way to illustrate the formation of hydrogen in the sub-surface can be addressed by the sequential H insertion [50]. We have investigated the occupation of H in the surface fcc sites and then on the sub-surface and positions closer to the bulk. In both cases, the H atoms sit at the octahedric sites. The average energy gained when adsorbing a monolayer of H atoms on the Pd surface is 0.54 eV/H atom. In the bulk, the average energy is lower, but still favorable as can be seen in Fig. 4. For the Pb@Pd system when the Pb atoms are on the surface, we have explored the adsorption in both the fcc involving Pd–Pb centers and those only formed by Pd. The fcc sites containing one Pb and two Pd do not efficiently adsorb hydrogen. The average adsorption energies for Pb@Pd are the following: the surface value corresponds to −0.53 eV/H atom and in the bulk −0.23 eV/H atom. These results agree very well with the observations performed by UHV experiments that indicated that the shape and maxima for the hydrogen evolution in a temperature-programmed desorption experiment is not significantly modified by the presence of Pb but instead it decreases the total amount of hydrogen adsorbed [51].

In order to address the effect of the solvent on the hydrogen uptake, we have employed the model for multilayer adsorption described in our previous work [9], see Fig. 5. The model states that the amount of hydrogen in the surface and bulk of Pd can be obtained as a particular case of multilayer adsorption [52]. For the clean Pd system, this means that at atmospheric pressures ($\log(p_{H2}/p^0) = 0$) the amount of hydrogen is larger than a single monolayer occupying the whole surface, $V/V_m > 1$, and then the hydride is formed. When the solvent is present, it modifies the effective pressure of hydrogen in contact with the catalyst due to solubility effects. In Fig. 5, it is shown how organic solvents (toluene and methanol) do reduce the total

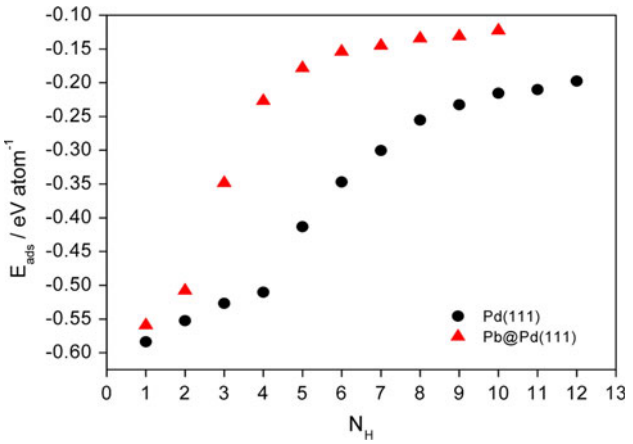

Fig. 4 Average adsorption energy, E_{ads} in eV/atom, for the adsorption of N_H hydrogen atoms in a $p(2 \times 2)$ supercell. *Black circles* represent Pd(111) and *red triangles* Pb@Pd(111). Notice that four H atoms are required to fill a monolayer in the Pd(111) case while for the Pb@Pd surface the two fcc positions in contact with the Pb site do not adsorb H

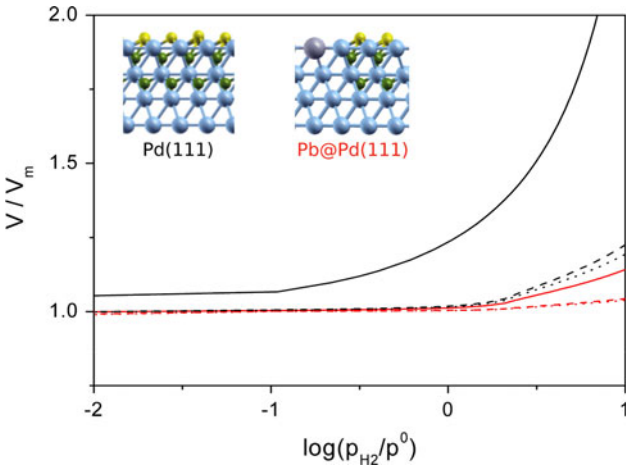

Fig. 5 Hydrogen volume uptake, V/V_m, as a function of the hydrogen pressure at 300 K considering different solvents. The *black lines* represent Pd and *red* Pb@Pd(111). *Solid lines* represent gas-phase models, *dashed lines* methanol and *dotted lines* toluene

hydrogen uptake when compared to gas-phase systems. In the case of the Pb@Pd alloy the resistance to form the hydride is increased even for the pure gas-phase system. Again, the effect of the solvent is to reducing hydride formation.

The formation of the carbide phase is controlled kinetically and competes with the formation of the hydride phase [9]. Carbide formation in sub-surface positions of Pd is −0.56 eV (with respect to gas-phase ethyne and H_2) and +0.58 eV (with respect to gas-phase ethene and H_2). As for the Pb@Pd alloy, the formation of the carbide is −0.25 eV (ethyne), 0.89 eV (ethene). Thus, Pb@Pd(111) is less prone to form the carbide phase than pure Pd.

3.3 Quinoline adsorption on Pd and Pb@Pd

Quinoline is a base with a naphtalene structure where one of the CH group has been substituted by nitrogen, see Fig. 6. The rings are planar and the N atom exhibits a lone pair sticking out from the carbon ring. In previous theoretical works [53], adsorption of quinoline has been studied by employing cluster models and different metals including Pd. These authors performed an extensive survey of different adsorption sites and indicated that the most likely positions for adsorption correspond to planar structures where the quinoline rings are over bridge positions (di-bridge configuration). In this configuration, the carbon and nitrogen are bonded in total to seven Pd atoms (this site was noted as di-bridge ($N_{Pd} = 7$) in Ref. [53]). Obviously, given the confined characteristics of the cluster and the poor definition of the *s*-bands in these models, the energies reported seem to be much smaller than those determined experimentally [54]. Another difficulty in the evaluation of quinoline adsorption comprises the large contributions that can be anticipated from its close nature and extended π-system. We have attempted to evaluate the contributions from dispersion through Grimme-like corrections [55] and reoptimized the structure. Those contributions have been reported to strongly modify the adsorption energies of large molecules [56]. In the case of quinoline on Pd, an extra exothermic contribution of 0.12 eV was obtained.

The perpendicular N-down structure was found unstable. The largest adsorption energies for quinoline on Pd correspond to the di-bridge site, −1.79 eV, see Table 2 and Fig. 6. The average distance from the carbon atoms in the rings to the neighboring metal atoms is 2.233 Å, while the distance from the N atom to a Pd on the surface is at 2.187 Å from the surface. The average C–C distances are enlarged to 1.447 Å with respect to the gas-phase values (1.421 Å). This enlargement is due to the formation of the bond at the interface.

Regarding the adsorption on the Pb@Pd model system, the number of adsorption possibilities increases due to the presence of different sites. We have calculated two different Pb concentrations on the surface. While at high Pb

Table 2 Adsorption site, adsorption energy, E_{ads} in eV, and most relevant geometric parameters, distance from the surface to the N atom in the quinoline, $d_{N–M}$; and from the metal ring to the neighboring metal atoms $d_{C–M}$; and average C–C distance, $d_{C–C}$; and α the angle for the distortion with respect to planarity. All distances in Å and α in °

	Pb/ML	Site	E_{ads}	$d_{N–M}$	$d_{C–C}$	$d_{C–M}$	α
Pd	0	Di-bridge	−1.79	2.187	1.447	2.233	20.8
Pb@Pd	0.25	Di-bridge	0.41	2.541	1.421	2.640	5.7
Pb@Pd	0.0625	Di-bridge	−1.57	2.203	1.446	2.248	22.3

concentration (0.25 ML) adsorption is endothermic by 0.41 eV, an exothermic value is obtained for lower Pb coverages, 0.0625 ML. In this case, the most stable adsorption site corresponds to position where quinoline is far away from the Pb atoms [di-bridge ($N_{Pd} = 7$)]. At Pb positions or close to these centers, adsorption energy is endothermic. Thus, the Pb centers are not decorated by the quinoline molecules. Instead, the clean Pd areas of the Pb@Pd alloys do adsorb quinoline in similar configurations as those found for the clean surface, thereby covering different areas of the catalyst where Pb is not present. The adsorption energies Pb@Pd are reduced to −1.57 eV. The projected density of states in Fig. 7 shows the important overlap between the states of the molecule and those of the surface, responsible for the strong interaction found. Moreover, the Pd atoms on the surface not close to the quinoline molecule are not significantly perturbed.

The role of quinoline appears to be, at least partially, equivalent to that of CO on Pd in the gas-phase alkyne hydrogenation. Both quinoline and CO have binding energies to the Pd or Pb@Pd surfaces that are larger than that of the triple C–C bond. This means that they are not displaced by the reactants but instead, they block some of the sites. This size reduction implies that the reaction ensembles (i.e., the group of atoms involved in an elementary step) are effectively reduced. Ensembles are known to rule activity and selectivity [57, 58] and their size reduction is particularly effective when the competing reactions require different ensembles, as for the hydrogenation and oligomerization processes, and the desired reaction needs the smallest one. In the case of quinoline, the large size of this molecule favors the isolation of small ensembles. Isolation also contributes to the reduction of oligomerization reactions as diffusion of alkynes on the surface is required and it is hindered when other adsorbates are present.

In order to check the role of other potential compounds on this reaction, we have analyzed the binding energy of pyridine and naphtalene to Pd. While the first contains a part of the active molecule, the second, $C_{10}H_{10}$ is isostructural with quinoline and with a CH group substituting N. The corresponding adsorption energies to the clean surface are found to be −1.14 eV (pyridine) and −1.84 eV (naphtalene). Thus, pyridine is much less adsorbed than both naphtalene and quinoline.

3.4 Thermodynamic factors of ethyne and ethene on Pd and Pb@Pd

One of the major components controlling the selective hydrogenation is known as the thermodynamic factor. This represents the ability of the catalysts to adsorb the alkyne while the alkene is not bonded [59]. However, the adsorption of the alkyne–alkene pair depends on the binding energy of carbon due to the bond-order conservation rules [60, 61]. The slope of the linear dependence found for the binding energies of alkyne and alkenes with that of carbon, points out where selective regions exist. However, this parameter is only valid provided that the same active species is responsible for the hydrogenation.

On the clean surface, the adsorption energies of ethyne and ethene are −1.78 and −0.82 eV, respectively. Thus, once formed the alkene stays adsorbed on the system that can be over-hydrogenated leading to the corresponding alkanes. For the clean surface, earlier experiments and calculations at stoichiometric conditions (H_2/alkyne = 1) lead to less than 50% selectivity for the partial hydrogenation. On the Pd–Pb sites, adsorption is controlled by the relative position with respect to the Pb center. Adsorption at the Pd fcc sites on the surface is less exothermic than on the pure Pd surface, the adsorption energy is −1.11 and −0.30 eV for ethyne and ethene, respectively. This was calculated in a $p(2 \times 2)$ reconstruction with a Pb coverage of 0.25 ML. Thus, the effect of alloying is to reduce the adsorption energies of both moieties by about 0.5–0.7 eV. At the fcc or bridge structures containing a Pb atom, the binding energies are even lower, thus the positions around Pb atoms can be considered as inactive. These results confirm the suggestion by Palczewska et al. [51] that with a very low Pb coverage, adsorbed ethene was not detectable in the TPD spectra and disappeared completely at higher coverages. The change of the metal–molecule bond strength was more decisive than site blocking [62]. When Pd is partially covered by quinoline, the binding energies are also smaller than those corresponding to the clean Pd surface. The E_{ads} is then −1.46 and −0.65 eV for ethyne

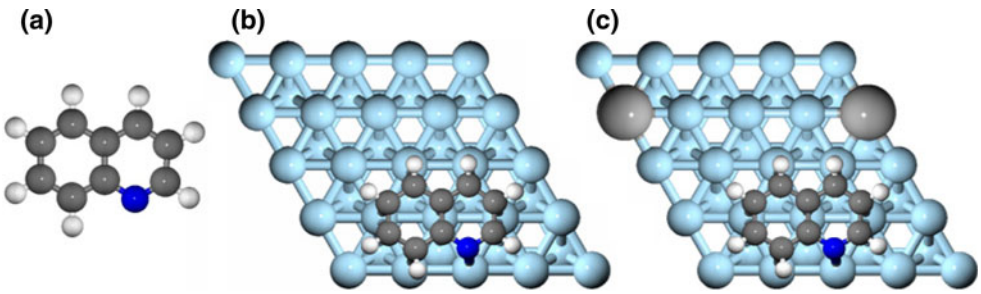

Fig. 6 Structures of **a** gas-phase quinoline and quinoline adsorbed on the surfaces: **b** di-bridge position on Pd and **c** di-bridge configuration at the Pb@Pd(111) surface. Color code: N (*dark blue*), C (*small gray*), H (*white*), Pd (*light blue*), and Pb (*large gray*)

Table 3 Reaction energies, ΔE, and activation barrier, E_a, both in eV, for the first and the second hydrogenation steps of ethyne

System	Pd		Pd–Q		Pb@Pd (c)		Pb@Pd (f)		Pb@Pd–Q_{Pd}	
Reaction	ΔE	E_a	ΔE	E_a	ΔE	E_a	ΔE	E_a	ΔE	E_a
$C_2H_2 + H \rightarrow C_2H_3$	−0.17	0.66	0.14	1.28	0.13	1.24	0.11	1.17	0.12	1.20
$C_2H_3 + H \rightarrow C_2H_4$	−0.42	0.81	−0.38	0.76	−0.28	0.90	−0.25	0.87	−0.45	0.72

For the Pb@Pd alloy (0.0625 ML Pb), two different structures: close (c) and far (f) from Pb have been studied

and ethene, respectively. Thus, quinoline also reduces the adsorption of the double and triple bonds to the surface, but the effect is smaller than that of Pb. In the large cell, we have also placed simultaneously quinoline and Pb, Pd@Pd–Q_{Pd}. On this system, the alkyne–alkene adsorption energies are reduced further (−1.35 and −0.61 eV, respectively) but still the synergetic contribution of quinoline and Pb is rather small.

3.5 Kinetics of ethyne and ethene hydrogenation on the Lindlar catalyst

Hydrogenation of unsaturated organic moieties takes place through the sequential addition of H atoms. This scheme is known as the Horiuti–Polanyi mechanism [63] and has been confirmed through computational DFT-based studies by Neurock et al. [7]. The reaction network for the hydrogenation of ethyne is known to show a branching point when vinyl can convert to ethene or to ethylidene. We have addressed this point previously [9], and found that conversion to ethylidene is particularly important for hydride phases. Given the results in the previous section with respect to the formation of hydrides, we have focused on the calculation of the reaction energies and kinetic parameters for the first and second hydrogenation steps leading to C_2H_3 and C_2H_4. The systems chosen are a Pd clean surface, and the Pb@Pd alloy with and without quinoline. The two calculated reactions were:

$$HC \equiv CH + H \rightarrow HC = CH_2 \quad (5)$$

$$HC = CH_2 + H \rightarrow H_2C = CH_2 \quad (6)$$

For the palladium surface, the first hydrogenation is exothermic by 0.2 eV, and the barrier is about 0.7 eV. Formation of ethene has an activation energy of 0.8 eV, see Table 3 and Fig. 8. When Pb is present, we have calculated two different configurations, either close (c) or far (f) from the Pb atom. The activation energy for the first step is then higher than for the clean Pd surface, about 1.2 eV, while the second hydrogenation requires less energy, about 0.9 eV. Therefore, although the barriers do increase from the Pd case, the energies are low enough for the first hydrogenation to take place at room or slightly higher temperatures. For the system containing quinoline Pd–Q, the first hydrogenation barrier is similar to that found for Pb@Pd, i.e., close to 1.3 eV, but the second hydrogenation is less energy demanding, 0.76 eV. Finally, for the whole system, Pb@Pd–Q_{Pd} with the quinoline adsorbed on the Pd region, the barriers are very similar to those of the quinoline alone: 1.2 and 0.7 eV for the first and second hydrogenations, respectively (see Fig. 8). If alkenes are adsorbed on the Pb@Pd–Q_{Pd} system, the hydrogenation barrier would be similar to those of previous steps ($E_a > 0.7$ eV) thus, the hydrogenation process would not compete with the fast desorption, $E_{des} = 0.6$ eV.

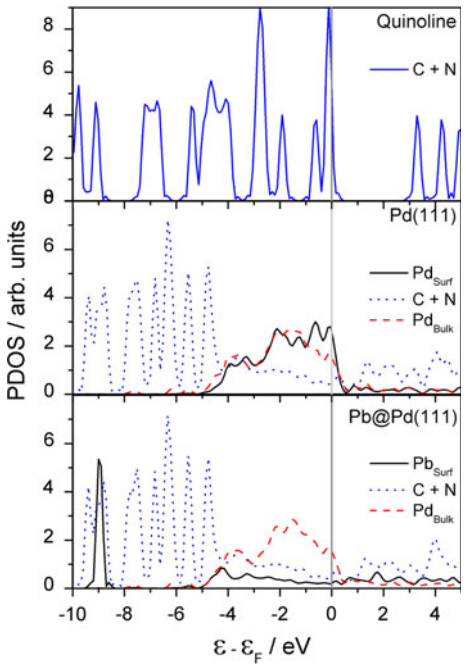

Fig. 7 Projected density of states for the most stable adsorption sites of quinoline on the Pd and Pb@Pd surfaces

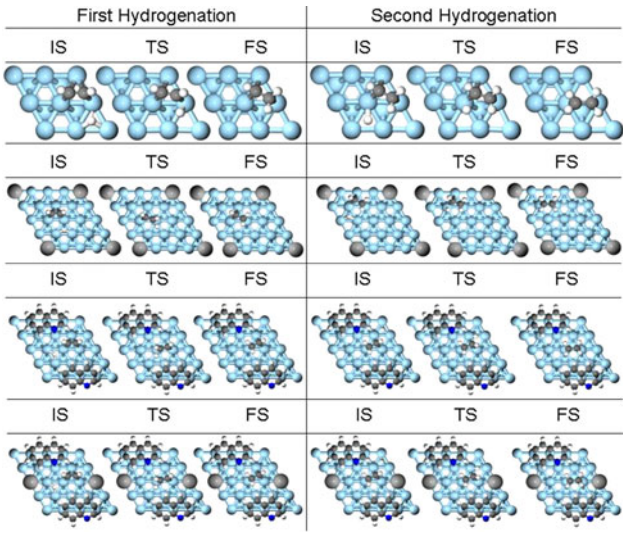

Fig. 8 Hydrogenation process on the clean Pd(111) surface; Pb@Pd alloy; quinoline adsorbed on Pd: Pd–Q; and Pb@Pd–Q_{Pd} Lindlar catalyst. The images show the initial, transition and final steps for each of the elementary steps. *Small white spheres* represent H, *small gray* C, *dark blue* N, *blue* Pd, and *large gray* Pb

4 Discussion: differences between palladium and the Lindlar catalyst

In the literature, selectivity modifiers have been classified in terms of reversible and irreversible adsorbates. Irreversible modifiers perturb the ensembles restricting their shape and size, while reversible adsorbates are usually seen as stoppers of consecutive over-hydrogenation or oligomerization reactions, in particular when the binding energy of the modifier is larger than that of the intermediate (thermodynamic selectivity) [64]. In the present section, we describe the effect of the irreversible (Pb) and reversible (quinoline) modifiers.

On regular Pd catalyst, H_2 is easily dissociated with the subsequent formation of hydrides. When hydrides are formed, ethyne (more generally, alkynes), over-hydrogenate due to the high chemical potential of H atoms stored in the Pd bulk. In the Lindlar catalysts, hydrides are scarcer. Still, H_2 splitting is easy due to the similar activity of Pd, but the presence of Pb inhibits the adsorption of H in the neighboring region. This exclusion area also implies that hydride formation is less exothermic and less likely. Moreover, the solvent modulates the amount of hydrogen in contact with the surface due to the solubility of H_2 in different liquids reducing the equivalent pressure. Thus, for the Lindlar catalyst over-hydrogenation problem is much less an issue. The role of the irreversible modifier is to reduce the sites available for hydrogen adsorption, isolate and shape the ensembles, and enhance the intrinsic selectivity of the catalyst by improving the thermodynamic factor. Finally, due to the Pb decoration at steps, carbon deposits are less likely.

Quinoline adsorption on Pd also reduces the amount of possible adsorption sites for H. This is due to the effective blocking of these molecules that adsorb so strongly that can compete with the alkyne for the sites. The presence of quinoline slightly reduces the average H binding energy. Furthermore, isolation of the sites is a clear effect of quinoline, its large size and quite good fitting with the symmetry of the surface allows the reduction of side reactions. However, quinoline is not as effective as Pb in improving the thermodynamic factor. For the complete Pb@Pd–Q_{Pd} system, the thermodynamic factor is similar to that observed for the quinoline alone.

Therefore, a hierarchical ordering on the effect of modifiers [65] can be obtained from the calculations above. A two-dimensional tessellation problem with two kinds of building blocks is described in Fig. 9. The Pb exclusion area forms the main modifier to the catalyst. Still, Pb is an additive that modifies very strongly the properties of adsorbed alkynes and alkenes and indeed it can completely block the surface, provided that an excessive quantity is employed. Moreover, Pb in the Pd alloys is preferentially found isolated. The reversible adsorbate quinoline is indirectly ordered by the presence of Pb and isolates very small sites of about four Pd atoms that allow hydrogenation but block oligomerization. Thus, at complete quinoline coverage the Pb@Pd–Q_{Pd} leaves active less than 10% of the surface palladium sites for the hydrogenation reaction. This fact, together with the smaller intrinsic activity (larger activation barriers for hydrogenation are found) explains why two orders of magnitude more Pd weight percentage is required in the formulations of the Lindlar catalyst when

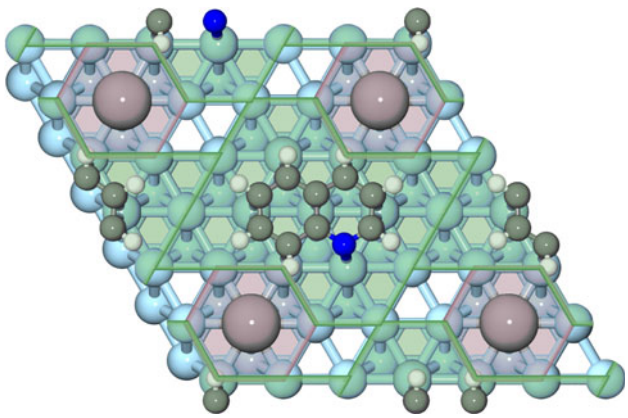

Fig. 9 Schematic representation of the mosaic generated by the superposition of the Pb exclusion areas (*pink*) and the quinoline ones (*gray*). The only active sites, without tiling, able to adsorb the alkyne are marked by white regions. The tessellation with two different kinds of structures provides a subtle way to control the ensemble size and shape

Table 4 Adsorption energies of ethyne and ethene on both Pd(111) and Pb@Pd(111) surface with and without quinoline

	System	Pb(ML)	Quinoline	Site	E_{ads}	d_{C-M}	$e_{\alpha-\beta}$
C_2H_2	Pd	–	No	Fcc	−1.78	2.001	0.153
C_2H_4	Pd	–	No	Bridge	−0.82	2.131	0.117
C_2H_2	Pb@Pd	0.25	No	Fcc	−1.11	2.055	0.135
C_2H_4	Pb@Pd	0.25	No	Bridge	−0.30	2.164	0.110
C_2H_2	Pd	–	Yes	Bridge	−1.46	2.255	0.041
C_2H_4	Pd	–	Yes	Bridge	−0.65	2.241	0.041
C_2H_2	Pb@Pd	0.0625	Yes	Fcc	−1.35	2.255	0.039
C_2H_4	Pb@Pd	0.0625	Yes	Bridge	−0.61	2.253	0.040

Energies are expressed in eV and distances in Å. The elongation, $e_{\alpha-\beta}$ in Å, is the difference between the C–C distance as calculated on the surface and in the gas phase

compared to the gas-phase hydrogenation, Table 1. Finally, the outstanding selectivity of the Lindlar catalyst would be difficult to be obtained by a single chemical modifier. The effect of Pb poisoning is too important (as shown in Table 4) that can eliminate all the active sites on the surface even at moderate coverages. Similarly, quinoline on Pd alone could also form very dense packing motives reducing the number of sites. By employing a hierarchically ordered set of modifiers (lead and quinoline) these problems are avoided as the two building blocks are different but complementary enough to limit the drawbacks of each other.

A second question is why different reversible modifiers are employed in gas-phase (CO) and three-phase (quinoline) hydrogenation. CO is widely employed in hydrogenations and indeed the catalyst is not selective without it in gas-phase reactions. In the Lindlar catalyst, quinoline is regarded as one of the most effective modifier. Both CO and quinoline show larger binding energies to the surface than ethyne, and therefore they both fulfill the requirement of improving the thermodynamic factor and not been replaced by the reactant. However, the coverage of both species is necessarily different; while a very dense CO layer is observed for CO a sparse structure is obtained with quinoline. Therefore, both do modify the ensembles but through different mechanisms: highly occupation by small molecule (CO) or large blocking by size (quinoline). However, CO might show solubility problems in the liquids, and it is dangerous to handle in an open environment, and the shape of the active sites is difficult to control. Therefore, it is not recommended in standard fine chemistry procedures. Similarly, N-containing compounds shall be removed from the streams in gas-phase hydrogenation due to incompatibilities with other parts of the process. Finally, we have tried different alternative molecules to investigate this effect. Naphtalene is one of them and its adsorption properties are similar to those obtained with quinoline. In contrast, pyridine is not an option as its low binding energy to Pd and Pb@Pd would not be enough to block the surfaces (i.e., it would be displaced by the alkyne).

5 Conclusions

We have employed DFT to investigate the roles of the different components in the Lindlar catalyst and compare them to palladium catalyst. Selective catalyst need to show three positive contributions: high thermodynamic factor (i.e., high alkyne adsorption and low alkene binding energies), they should not generate hydrides (as hydrides over-hydrogenate) and should not promote the formation for oligomers through C–C coupling. In the Lindlar catalyst, DFT shows that this is achieved as follows:

1. Pd is active in both H_2 splitting and hydrogenation. However, both over-hydrogenation and oligomerization limit the selectivity of the catalyst.
2. The exceedingly large ability of Pd to form palladium hydrides is partially modulated by the presence of Pb that reduces the overall amount of H in the catalyst.
3. The solvent also helps in reducing the effective H_2 pressure on the surface as it is modulated by the gas solubility in the liquid phase.
4. Pb improves the thermodynamic factor as alkene adsorption is strongly reduced when significant amounts of Pb are present.
5. Quinoline basically acts by blocking possible H and alkyne adsorption sites. The isolation of the active centers is beneficial as it impedes the formation of C–C bonds (i.e., oligomerization).

In summary, we have analyzed by means of first principle studies the fundamental role of all the components in the Lindlar catalyst. This is the first time that an extensive computational approach is devoted to understand at the molecular level this famous catalyst that has been successfully employed in industry for nearly 6 decades.

Acknowledgments We thank MICINN for Grants CTQ2009-07753/BQU and CSD2006-0003 and BSC-RES for providing generous computational resources.

References

1. Somorjai GA, Borodko YG (2001) Catal Lett 76:1
2. Corma A, Serna P (2006) Science 313:33
3. Molnar A, Sarkany A, Varga M (2001) J Mol Catal A 173:185
4. Chorkendorff I, Niemantsverdriet HW (2003) Concepts of modern catalysis and kinetics. Wiley-VCH Verlag GMBH KGaA, Weinheim

5. García-Mota M, Cabello N, Maseras F, Echavarren AM, Pérez-Ramírez J, López N (2008) Chem Phys Chem 9:1624
6. Plata JJ, García-Mota M, Braga AAC, Maseras F, López N (2009) J Phys Chem A 113:11758
7. Mei DH, Sheth PA, Neurock M, Smith CM (2006) J Catal 242:1
8. Mei DH, Neurock M, Smith CM (2009) J Catal 268:181
9. García-Mota M, Bridier B, Pérez-Ramírez J, López N (2010) J Catal 273:92
10. Studt F, Abild-Pedersen F, Bligaard T, Sorensen RZ, Christensen CH, Nørskov JK (2008) Science 320:1320
11. Lindlar H (1952) Helv Chim Acta 35:446
12. Lindlar H, Dubuis R (1973) Org Synth 5:880
13. Mallat T, Baiker A (1991) Appl Catal 79:59
14. Stachurski J, Thomas JM (1988) Catal Lett 1:67
15. Massalski TB, Okamoto H, Subramanian PR, Kacprzak L (1990) Binary alloy phase diagrams. ASM International, Materials Park
16. Chadwick D, Karolewski MA (1983) Surf Sci 126:41
17. Liu G, Davis KA, Meier DC, Bagus PS, Goodman DW (2003) Phys Rev B 68:035406
18. Palczewska W, Szymerska I, Ratajczykowa I, Lipski M (1980) In: Proc ECOSS-3 and ICCS-4 Cannes
19. Szabo S (1991) Int Rev Phys Chem 10:207
20. Mallat T, Baiker A (1995) Top Catal 8:115
21. McEwen AB, Guttieri MJ, Maier WF, Laine RE, Shvo Y (1983) J Org Chem 48:4436
22. Mallat T, Baiker A (2000) App Catal A 200:3
23. Maier WF, Chettle SB, Rai RS, Thomas G (1986) J Am Chem Soc 108:2608
24. Yu J, Spencer JB (1998) Chem Commun 1103
25. Segura Y, López N, Pérez-Ramírez J (2007) J Catal 247:383
26. Bridier B, López N, Pérez-Ramírez J (2010) J Catal 269:80
27. Bridier B, Pérez-Ramírez J (2010) J Am Chem Soc 132:4321
28. Oroshnik W (1977) Synthesis of Vitamin A, intermediates and conversion thereof to Vitamin A "4058569"
29. Coq B, Figueras F (2001) J Mol Catal A 173:117
30. Kresse G, Joubert D (1999) Phys Rev B 59:1758
31. Perdew JP, Chevary A, Vosko SH, Jackson KA, Pederson MR, Singh DJ (1992) Phys Rev B 46:6671
32. Blochl PE (1994) Phys Rev B 50:17953
33. Monkhorst HJ, Pack JD (1976) Phys Rev B 12:5188
34. Henkelman G, Uberuaga BP, Jonsson H (2000) J Chem Phys 113:990
35. Soto-Verdugo V, Metiu H (2007) Surf Sci 601:5332
36. Ulan JG, Maier WF, Smith DA (1987) J Org Chem 52:3132
37. Ulan JG, Kuo E, Maier WF, Rai RS, Thomas G (1987) J Org Chem 52:3126
38. Schlogl R, Noack K, Zbinden H, Reller A (1987) Helv Chim Acta 70:627
39. Hammer B, Morikawa Y, Nørskov JK (1996) Phys Rev Lett 76:2141
40. Greenwood NN, Earnshaw A (2008) In: Chemistry of the elements, 2nd edn. Elsevier, p 1150
41. Knapton AG (1977) Plat Met Rev 21:44
42. Andersin J, López N, Honkala K (2009) J Phys Chem C 113:8278
43. Andersin J, Honkala K (2010) Surf Sci 604:762
44. Nykanen L, Andersin J, Honkala K (2010) Phys Rev B 81:075417
45. Seriani N, Mittendorfer F, Kresse G (2010) J Chem Phys 132:024711
46. Bond GC (2005) Springer, New York, p 395
47. Teschner D, Borsodi J, Wootsch A, Revay Z, Havecker M, Knop-Gericke A, Jackson SD, Schlogl R (2008) Science 320:86
48. Mitsui T, Rose MK, Fomin E, Ogletree DF, Salmeron M (2003) Nature 422:705
49. López N, Łodziana Z, Illas F, Salmeron M (2004) Phys Rev Lett 14:146103
50. Greeley J, Krekelberg WR, Mavrikakis M (2004) Angew Chem Int Ed 43:4296
51. Palczewska W, Ratajczykowa I, Szymerska I, Krawczyk M (1984). In: Proceedings of the 8th international congress on catalysis, Berlin, vol IV, p 713
52. Brunauer S, Emmett PH, Teller E (1938) J Am Chem Soc 60:309
53. Santarossa G, Iannuzzi M, Vargas A, Baiker A (2008) ChemPhysChem 9:401
54. Ulan GJ, Kuo E, Maier WF, Rai RS, Thomas G (1986) J Org Chem 52:3126
55. Grimme S (2006) J Comput Chem 27:1787
56. Mercurio G, McNellis ER, Martin I, Hagen S, Leyssner F, Soubatch S, Meyer J, Wolf M, Tegeder P, Tautz FS, Reuter K (2010) Phys Rev Lett 104:036102
57. Chen MS, Kumar D, Yi CW, Goodman DW (2005) Science 310:291
58. García-Mota M, López N (2008) J Am Chem Soc 130:14406
59. Jia JF, Haraki K, Kondo JN, Domen K, Tamaru K (2000) J Phys Chem B 104:11153
60. Studt F, Abild-Pedersen F, Bligaard T, Sørensen RZ, Christensen CH, Nørskov JK (2008) Angew Chem Int Ed 47:9299
61. Abild-Pedersen F, Greeley J, Studt F, Rossmeisl J, Munter TR, Moses PG, Skulason E, Bligaard T, Nørskov JK (2007) Phys Rev Lett 99:16105
62. Cerveny L, Paseka I, Surma K, Thanh NT, Ruzicka V (1985) Collect Czech Chem Commun 50:61
63. Horiuti J, Polanyi M (1934) Trans Faraday Soc 30:1164
64. Siegel S, Hawkins JA (1986) J Org Chem 51:1638
65. Anderson JA, Mellor J, Wells RPK (2009) J Catal 261:208